

Boosting Palladium Catalyzed Aryl–Nitro Bond Activation Reaction by Understanding the Electronic, Electrostatic and Polarization Effect: A Computational Study from Basic Understanding to Ligand Design

Yumiao Ma^{*a,b} and Zhaohong Wang^c

- BSJ Institute, Haidian, Beijing, 100084, People's Republic of China.
- Hangzhou Yanqu Information Technology Co., Ltd. Xihu District, Hangzhou City, Zhejiang Province, 310003, People's Republic of China.
- Department of Chemistry and Chemical Biology, Cornell University, Ithaca, NY 14853, United States.

Abstract

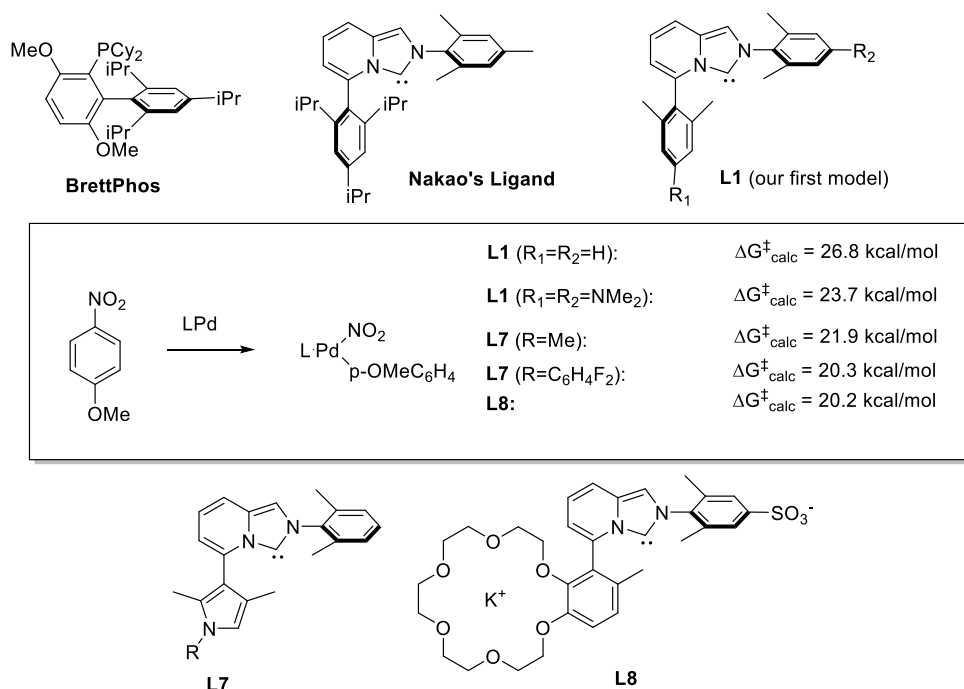
Although cross coupling reaction with nitroarene as the electrophilic partner has gained high interest recently, the palladium catalyzed aryl–nitro bond activation reaction still requires rather high temperature and harsh condition. In this work, based on Nakao's nitrogen heterocyclic carbene (NHC) ligand, we systematically explored the substituent effect on the oxidative addition step, the known rate determining step of the whole reaction, by density functional theory (DFT) calculation. The key aryl ring on the ligand skeleton, namely Ring A, acts as a π -donor and stabilizes the palladium center of the transition state, as shown by Extended Transition State Natural Orbital of Chemical Valance (ETS-NOCV) analysis, and thus an electron-rich Ring A is expected to lower the barrier. On the other hand, however, the polarization and electrostatic effects were shown to be as or even more important, although they were often ignored before. These effects originate from through-space interaction with the nitro group in the resting state, and the overall effect is that any polarizable or partly negative group nearby the *ortho*- or *meta*- site of Ring A is harmful for the reaction. Based on these discoveries, we proposed a list of guidelines for successful ligand development, and designed several new ligands. These ligands exhibit significantly lower barrier than the reported Nakao's ligand by as large as ~ 5 kcal/mol in both gas phase and solvation, and might be good candidates for further experimental study.

Introduction

Accompanied by the blossom of organometallic chemistry, transition metal catalyzed cross coupling has been one of the most important parts in current chemistry. The Ullmann¹, Buchwald-Hartwig², Heck³, Suzuki-Miyaura^{4, 5}, Hiyama⁶, Sonogashira⁷ and other cross coupling reactions have been well-developed and widely explored. In addition to these well-known reactions making use of halides as the electrophilic part, the activation of C–O⁸, C–S⁹, C–CN¹⁰ and other bonds^{11, 12} is also being developed in recent years, which has significantly expanded the substrate scope of cross coupling reactions. Among these new developments, the activation of aryl–nitro bond^{13, 14} is of high interest, due to the wide availability and versatility of nitroarenes¹⁵. Since 2010s, Nakao reported the Buchwald-Hartwig¹⁶ and Suzuki-Miyaura¹⁷ reaction promoted by BrettPhos-Pd complex. Besides, organocatalyzed activation of aryl–nitro bond has also been reported recently¹⁸. In 2019, Nakao reported another palladium-catalyzed cross coupling of nitroarene¹⁹, with a novel Nitrogen Heterocyclic Carbene (NHC)-Pd complex inspired by the structure of BrettPhos. With this catalytic system, the reaction efficiency was further increased. However, a harsh condition (130 degree, 12 h) is still required for a successful reaction. Obviously, further optimization of the catalyst is highly demanded to improve both the efficiency and mildness of nitroarene activation reaction.

In this work, based on Nakao's NHC ligand, we systematically explored the substituent effect on the NHC-Pd catalyzed aryl–nitro bond activation by DFT calculations. While electronic effect plays a role in determining the oxidative addition barrier, the electrostatic and polarization effect are as important, which might be often ignored in previous research. Based on our results, a guideline for further ligand optimization was proposed, and several new NHC ligands were designed, which were predicted to substantially improve the reactivity of NHC-Pd catalysts towards aryl–nitro bond activation.

(a)



(b)

Influential Factors

Dispersion

C1 to Pd donation

Polarization of R1

and C2,6

R1–NO₂Ar electrostatic

effect

Donation by R2

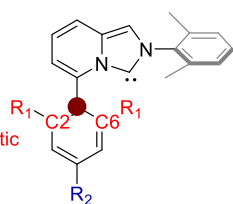
Design Rules

Ring B: stabilizing TS by dispersion
subtle substitution effect

C1, should be good π -donor

**R1, should be non-polarizable or δ^+
but should not be strongly positively
charged (important)**

R2, should be EDR



Scheme 1. (a) An overview of the previously studied and newly designed ligand in this work, as well as their calculated barrier for aryl–nitro bond oxidative addition of the corresponding Pd(0) complex. (b) The summary of the ligand design rule found in this work.

Results and Discussion

Basic Insights

In Nakao's article in 2017, a DFT calculation has been performed for the BrettPhos-Pd promoted cross coupling reaction with nitroarene as the electrophile, and it has been established that the oxidative addition (OA) of NHC-Pd(0) complex to the C–N bond is the rate-determining step. In

Nakao's report, the OA requires a barrier of 28.0 kcal/mol, leading to the demanding of a high reaction temperature of 130 °C. As a result, in this work we focus on the OA step of NHC-Pd(0) complex, and study the factors that influence the barrier. Because the solvent used experimentally for this reaction are generally of rather low dipole (e.g. heptane, or 1,4-dioxane), we firstly calculated the gas phase barriers to find a general trend, and then validated the robustness of our conclusions with some privileged ligands in a more polar solvent (THF).

As a starting point, we examined the Gibbs free energy profile for the OA of NHC-Pd(0) toward 4-nitroanisole, with **L1**(**R1=R2=H**) as the model. This model ligand was taken to simulate Nakao's ligand, with *i*Pr groups replaced by methyl groups. The active catalyst **L1Pd** forms π -complex with the substrate with large exothermity of -24.6 kcal/mol. Similar to BrettPhos, **L1** also interacts with the Pd atom with its aryl carbon C1 in addition to its NHC center, with a moderate C–Pd distance of 2.99 angstrom in **Int1**. This compound then undergoes the OA through **TS1**, with a barrier of 26.8 kcal/mol. There are two isomers of **TS1**, between which the dissociating nitro group prefers to be *cis* to C1 by a very little difference (0.2 kcal/mol). However, the preference is rapidly enlarged to be 7.1 kcal/mol in the planar 4-coordinated product **Int2**. Furthermore, in some of the other ligands studied in this work, **TS1** is favored over **TS1_Conf2** by a larger difference. We attributed this difference to the *trans*-influence²⁰: since the nitro group has a rather weak *trans*-influence ability as compared to the aryl group, the Pd–NHC bonding is less weakened when the nitro group is *trans* to the carbenoid carbon (i.e. in **Int2** and **TS2**), as reflected in the Pd–NHC distance (2.01 angstrom in **Int2** and 2.08 angstrom in **Int2_Conf2**). Due to its lower energy, all the **TS1** mentioned later refers to the isomer with nitro group *cis* to C1, if not specially noted.

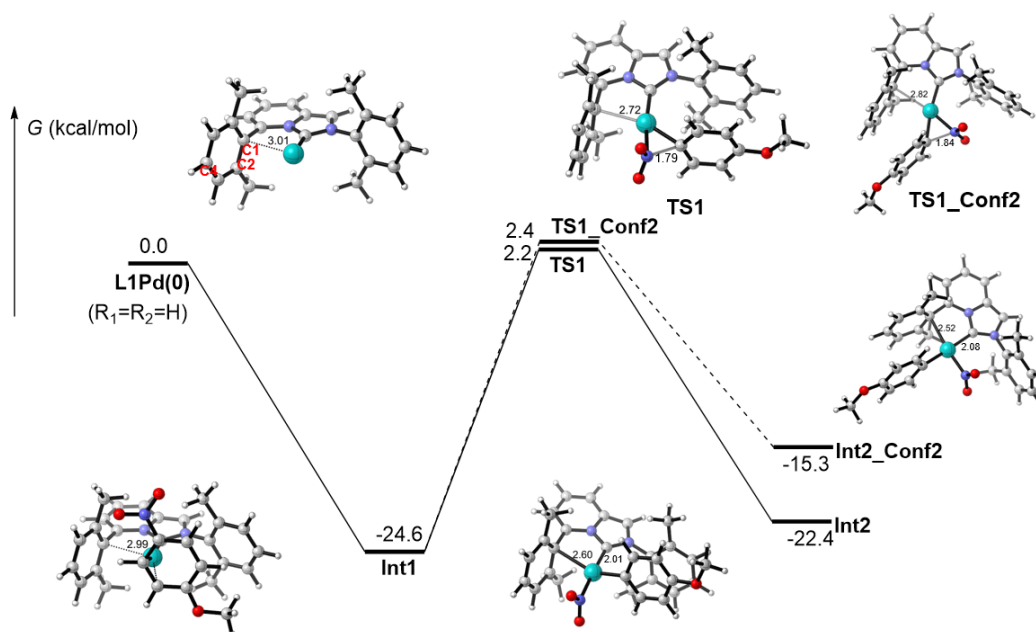


Figure 1. The Gibbs free energy profile for the OA reaction of **L1Pd** toward 4-nitroanisole. Distances are shown in angstrom.

Based on the energy profile above, we could clearly see that the OA of **L1Pd**(**R1=R2=H**) requires a high barrier (26.8 kcal/mol), which limits the efficiency of the catalysts. Notably, the Pd–C1

interaction is strengthened during the OA process: the Pd–C1 distance is reduced to 2.72 angstrom in **TS1**, and finally to 2.60 angstrom in **Int2**. Thus the aryl group is believed to stabilize the Pd(II) species through this complexation effect. Naturally, one may expect that the electronic property of this aryl ring could regular the reactivity. In order to explore the substituent group effect, we performed Hammett analysis²¹ based on **L1**, **L2** and **L3** (Figure 2).

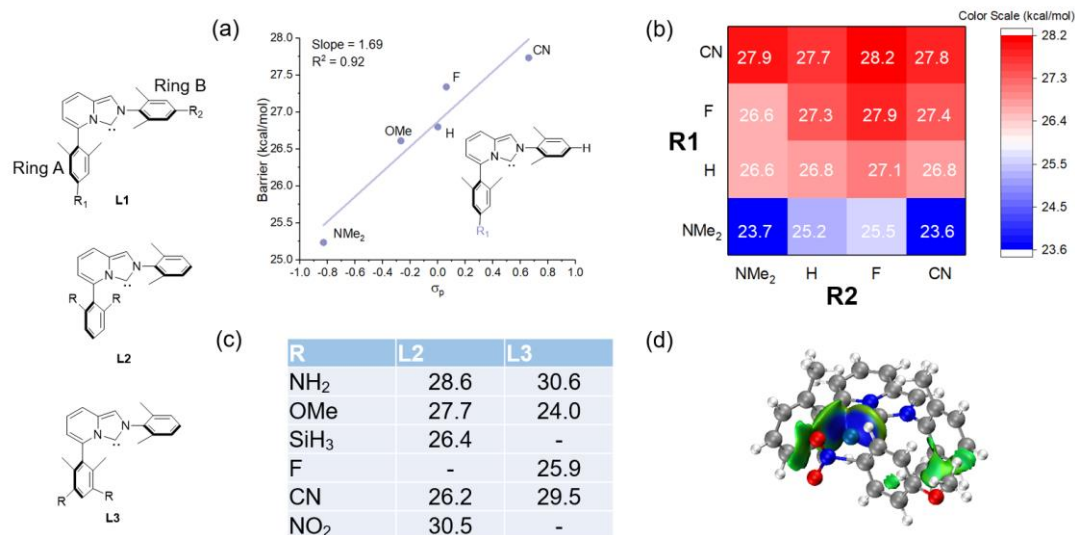


Figure 2. The structure for **L2** and **L3**, and (a) The Hammett relationship for **L1Pd** promoted OA reaction, (b) the barriers with various R1 and R2 for **L1Pd** promoted OA, (c) the barriers with various R for **L2Pd** and **L3Pd** promoted OA, (d) the IGM isosurface of **TS1** for **L1Pd** (R1=R2=H).

With **L1** as the model, the effect of para-substituent group on both the two phenyl rings was explored. The OA barrier exhibits good linear relationship with the para-Hammett constants on Ring A, showing that an electron-donating group at C4 promotes the reaction. On the other hand, the effect of substitution on Ring B is subtle (Figure 2b). We examined 16 ligands with various substituent groups R1 and R2, and found that both very electron-donating (NMe₂) and very electron-withdrawing (CN) R2 are able to lower the barrier by 1~2 kcal/mol, in comparison to H or F. The effect of R2 is proposed to originate from the dispersion interaction: although Ring B does not directly form chemical bonding with the Pd center, the substrate phenyl ring parallels Ring B, and π - π interaction is proposed to provide stabilization. The presence of dispersion interaction is evidenced by the Independent Gradient Model (IGM) analysis²², as shown in Figure 2d. The attractive dispersion interaction is clearly shown by the green area between the two phenyl groups. As this interaction is known to originate from charge transfer and polarization, it could be expected that R2 with strong electronic effect increases the polarizability of Ring B, and thus increase the dispersion stabilization.

According to the substituent group scanning in Figure 2b, we have found that ligand **L1** with R1=R2=NMe₂ could promote the OA of Pd(0) toward 4-nitroanisole with a barrier of 23.7 kcal/mol, much lower than the original ligand of 26.8 kcal/mol. It should be noted that although these Gibbs free energies were obtained at room temperature, since the barrier is determined by an intramolecular OA of **Int1**, the conclusion could be smoothly migrated to other temperature. As a result, it is predicted that **L1** (R1=R2=NMe₂) should give a reaction rate increase of ~65 fold at 100 °

C.

Then we turned to study the substituent effect of the *meta*- or *ortho*- substitution on Ring A (Figure 2c). Only substitute modes that does not strongly bother the steric property were studied. In Nakao's experimental report, the yield sharply decreased when the *ortho*-alkyl groups were replaced by alkoxy groups, which seems rather interesting considering the above data that *para*-electron donating groups (EDRs) facilitates the reaction. Although one may attribute this observation to other factors such as ligand stabilization, our calculations, however, show that *indeed* any *ortho*-substitutes rather than alkyl groups have minor or harmful impact on the barrier. For example, by replacing *ortho*-methyl to *ortho*-methoxy group, the barrier is raised to 27.7 kcal/mol, in consistence with Nakao's observation. The situation is similar for *meta*-substitution, for which only *meta*-methoxy group decreases the barrier by 1.8 kcal/mol, while the effects of all the groups examined are either harmful or negligible. This observation does not parallel in any known order of electronic effect, and is in sharp contrast to the *para*-substituent effect that EDRs promote the reaction. Then we have to answer the question on the origin of the diverse substituent effect.

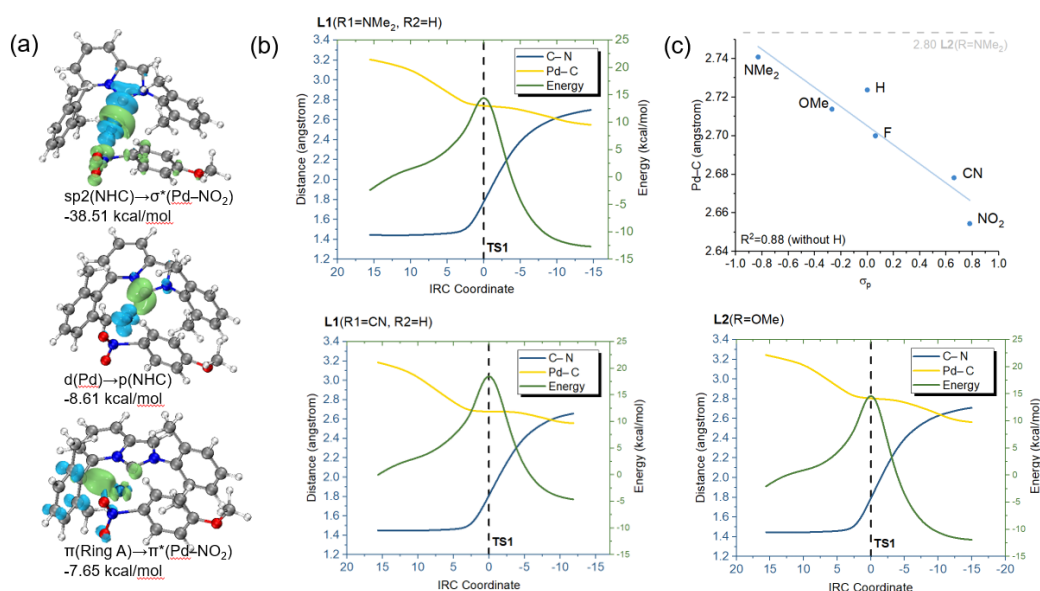


Figure 3. (a) The ETS-NOCV pair density isosurface (isovalue at 0.002) for the orbital interaction between Pd-substrate fragment and the NHC ligands. (b) The evolution of bond length and energy along the IRC path for $\text{TS1}(\text{L1})$ (R1=NMe₂, R2=H) and $\text{L1}(\text{R1}=\text{CN}, \text{R2}=\text{H})$. (c) The linear relationship between Pd-C1 distance and substituent group Hammett constant in $\text{TS1}(\text{L1})$, and the IRC profile for $\text{TS1}(\text{L2})$ (R=OMe).

First, Extended Transition State Natural Orbital of Chemical Valence (ETS-NOCV) analysis²³ was performed to study the nature of the interaction between Pd and Ring A. ETS-NOCV gives several pair densities, each representing one pair of orbital interaction between two fragments. The pair density isosurface for $\text{TS1}(\text{L1}, \text{R1}=\text{R2}=\text{H})$ is shown in Figure 3a, as well as their contribution to total energy. The donor and acceptor orbitals were colored as blue and green, respectively. Clearly, the NHC-Pd donation and backdonation contributes most of the interaction energy, and of special interest is the third pair, in which the occupied orbital on Ring A centered at C1 is donated to the antibonding Pd-NO₂ orbital. This observation is in consistence with the general knowledge that

BrettPhos-like ligands stabilize the Pd(II) species by aryl donation. According to this result, one should obviously expect that an electron-rich Ring A gives stronger donation to the Pd(II) center in **TS1** and thus lowers the barrier, which is the case for *para*-substitution. But, what about the *ortho*- or *meta*- substitution? Why almost all substituent groups raise the barrier?

In order to answer this question, we compared the Intrinsic Reaction Coordinate (IRC) profile and the evolution of key distances. Interestingly, although one might expect that an electron-rich Ring A binds stronger with the Pd atom being oxidized, **TS1(L1(R1=CN,R2=H))** exhibits shorter Pd–C1 distance as compared to its NMe₂ analogue (2.68 versus 2.71 angstrom). On the other hand, the Pd–C1 distances in the OA product **Int2** are almost the same. However, this does not mean that *para*-nitrile stabilize **TS1** more efficiently: the bond length in TS depends on the position of TS on the reaction coordinate; it is the result of the development of various interactions, but not their cause. By comparing the IRC profile, we found that the 4-CN TS occurs later than its 4-NMe₂ analogue. For example, starting from **Int1**, the Pd–C1 distance is shortened by 14% in **TS1(L1(R1=NMe₂, R2=H))**, and the value is 16% for **TS1(L1(R1=CN, R2=H))**. The later TS indicates that the electron-deficient Ring A provides less stabilization to the Pd(II) center at the same distance, and thus closer contact is required to reach the TS.

The above trend is more clearly shown in Figure 3c by plotting Hammett constant with the Pd–C1 distance of a series of **TS1(L1(R2=H))**, with only R1=H as an outlier. It could be summarized that a stronger EDR at *para*-site leads to the longer Pd–C1 distance in **TS1**, and the lowers the barrier. Interestingly, if we put the line representing the Pd–C1 distance in **TS1(L2(R=OMe))** in this plot (2.80 angstrom), it lies even higher than the strongest EDR in this work, i.e. NMe₂. As a result, if the substituent group-geometry relationship is kept for *ortho*-substitution, **L2(R=OMe)** should have a rather electron-rich aryl group. Furthermore, by considering the IRC profile, it could also be seen that the profile of **L2(R=OMe)** is rather similar to **L1(R1=NMe₂, R2=H)**. All these observations suggest that *ortho*-methoxyl substituted ligand should have a rather high activity, which is in sharp contrast to the barrier value. As a result, the high barrier for *ortho*-substituted ligand must come from the resting state (**Int1**) stabilization, instead of transition state destabilization.

At the first glance, the **Int1** stabilization effect for *ortho*- substitution seems rather weird, since there is only minor chemical bonding between Ring A and Pd in **Int1** as compared to **TS1**. However, according to the observation that almost any *ortho*-group raises the barrier, we suggest that it is some yet-unknown electrostatic- or field-originated effect that dominates this reaction. In order to study this effect, we made a density difference isosurface for the key species. This isosurface is obtained by extracting the electron density of the ligand, the Pd atom, and the nitroarene part from the whole molecule, and thus the electron transfer upon formation of the complex can be seen (Figure 4). Interestingly, although the *ortho*-substituent group (methyl group in Figure 4) does not bind to Pd in any manner, significant polarization happens upon the formation of **Int1**. The loss of electron density from the side near the nitro group of Ring A can be clearly seen from the blue surface, which could be attributed to be the polarization effect of the strong dipole introduced by the nitro group. This polarization disappears in **TS1** as the nitro group is no longer oriented toward the *ortho*- substituent group: there is no significant density reformation on the *ortho*-site then, but the slight electron density loss is remained at the *meta*-site. According to this observation, it can be

inferred that any *ortho*-substituent group that is polarizable, or prior to donate its electron density, should stabilize **Int1**, but this stabilization effect is ceased in **TS1**. Since almost all the substituent groups rather than alkyl have polarizable π - or n- electron, it is understandable that almost all *ortho*-groups increase that barrier through this polarization effect. The trend in barrier value shows that this effect is so strong that the conventional electronic effect through aryl conjugation is overridden.

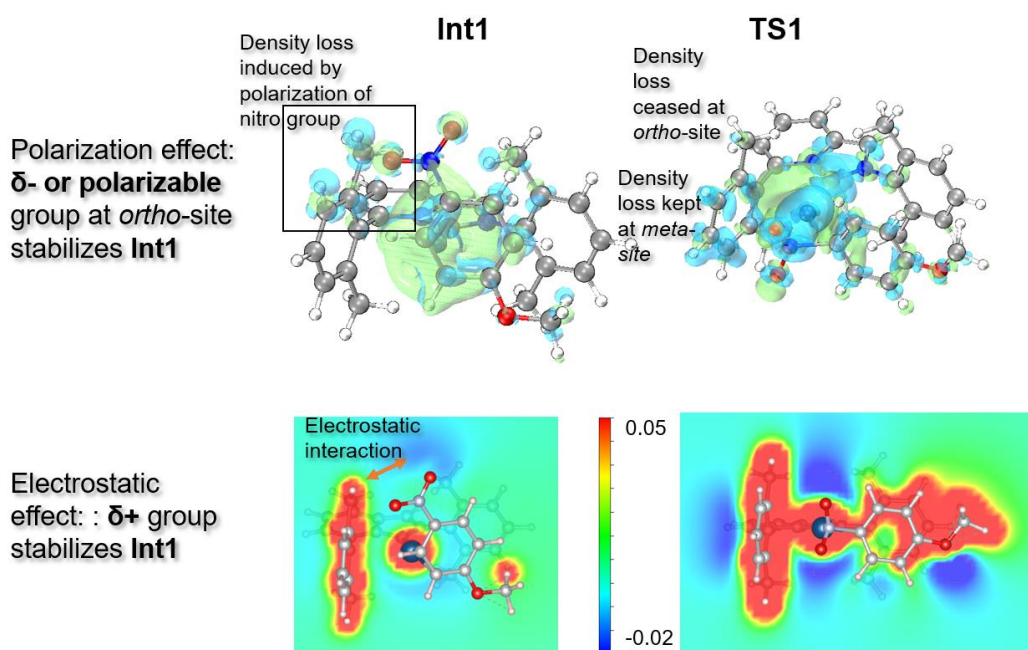


Figure 4. (top) The density difference isosurface (at isovalue of 0.001) of **Int1** and **TS1** with **L1**(R1=R2=H) as the ligand. Blue and green areas represent the loss and accumulation of density upon complexation respectively. (bottom) The 2D colored mapped contour for the electrostatic potential (ESP).

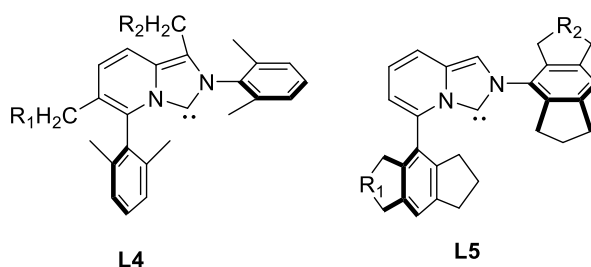
This polarization effect is also in the opposite direction to the electrostatic effect. Since the nitro oxygen atom is known to exhibit negative charge, positively charged *ortho*-group is expected to stabilize **Int1** through electrostatic effect (the negative electrostatic potential nearby the nitro group is shown in the bottom part of Figure 4). However, a positively charged group is difficult to bear density loss shown in the top part of Figure 4. Both the two effects should contribute to the overall energetics, and the electrostatic effect is proposed to be competed out in the cases studied above.

In a summary, in this part we have studied the substituent effect at the *ortho*-, *meta*- and *para*- site of Ring A. While the effect of *para*-substitution well parallels its electron donating ability, the *para*- and *ortho*- substituent effect originates from much more complicated factors. The nitro group in **Int1** strongly polarize both the *ortho*- and *meta*- site, leading to the electron density loss at these positions, and thus any polarizable group or group prone to donate its electron will raise the OA barrier through this resting state stabilization effect. On the other hand, the negatively charged nitro oxygen in **Int1** prefers interacting with a partial positive *ortho*- group through an electrostatic manner. These factors, as well as the conventional electronic effect through aryl ring A, contributed

to the final energetics.

Ligand Design

Based on the understanding established above, we are able to design some new ligands and further validate the conclusion about polarization effect. Since the polarization effect leads to electron density loss on the *ortho*-substituent groups of **L1** in the resting state **Int1**, we propose that the introduction of a (partial) positive charged group will prevent this unwanted resting state stabilization. In the following part, we present the ligand design as the proof-of-concept.



L4		
R1	R2	Barrier (kcal/mol)
H	H	25.7
NH ₃ ⁺	H	28.0
H	NH ₃ ⁺	26.5
BF ₃ ⁻	H	25.8
NH ₃ ⁺	BF ₃ ⁻	27.7
BF ₃ ⁻	NH ₃ ⁺	23.8
L5		
R1	R2	Barrier (kcal/mol)
CH ₂	CH ₂	27.3
NMe ₂ ⁺	CH ₂	28.5
BF ₂ ⁻	CH ₂	31.8
CH ₂	NMe ₂ ⁺	27.0
CH ₂	BF ₂ ⁻	22.6

Table 1. OA barrier with ligands **L4** and **L5**.

The ligand **L4** represents a family of imaginary molecules, in which charged groups NH₃⁺ or BF₃⁻ are placed on the back side of Ring A and Ring B, near the center position of the ring, instead of the *ortho*- site (Figure 5). Various combinations of charge groups were tested, and no improvement was gained except for the **L4**(R1=BF₃⁻, R2=NH₃⁺), which could be attributed to the orientated electric field generated by the zwitterion-type ligand. The failure of **L4** confirmed the observed substituent effect with spatial position requirement that the substitution must be placed nearby the *ortho*- site, in consistence with our polarization model. Then we tested the **L5** family, which are potentially synthetically available. In this family, charged groups are places around the phenyl rings with a cyclopentane motif. Unfortunately, the introduction of tetraalkylammonium motif at Ring A leads to no barrier decrease, because of the formation of a rather stable **Int1** due to charge interaction with the nitro oxygen (Figure 5). In this case, the electrostatic effect outcompetes the polarization effect

due to the presence of strong positive charge.

Although the trials with **L4** and **L5** family gave no practical useful results, the following two families, **L6** and **L7** showed rather interesting behavior. **L6** was designed to make use of azulene, the non-benzene aromatic ring with intrinsic dipole. By placing the cationic side of azulene as Ring A, the OA barrier was lowered to 25.3 kcal/mol, much lower than its analogue with similar steric property (**L6Np**, 29.7 kcal/mol). We believe that the cationic nature introduced into Ring A site by azulene decreased the polarization-based resting-state stabilization, and led to the barrier lowering effect.

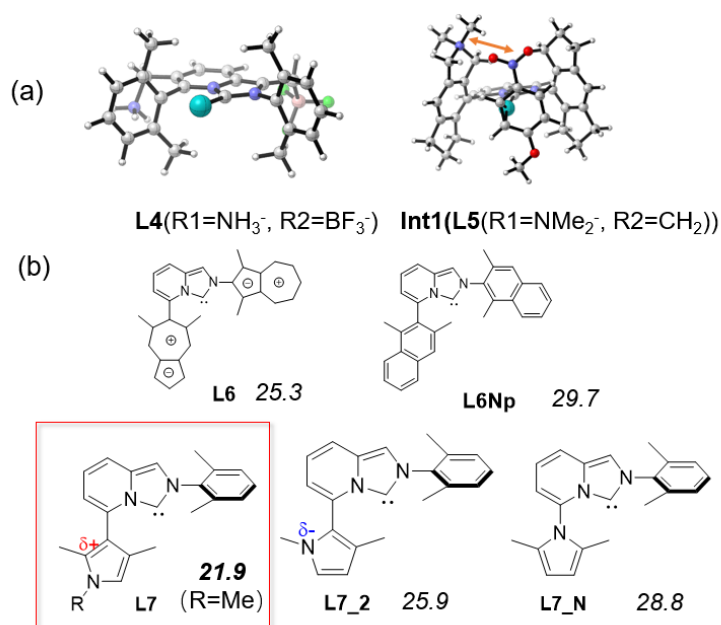


Figure 5. (a) The geometry of **L4Pd** and **Int1(L5)** with selected substitution mode. (b) The structure of **L6** and **L7**.

Another even more practically useful ligand was designed based on pyrrole ring as Ring A. It is known that pyrrole ring is electron-rich with its HOMO distributed on C2 and C3, but not the nitrogen. The electron-richness leads pyrrole motif to be an excellent Pd(II) stabilizer. Furthermore, the presence nitrogen atom leads C2 of pyrrole to exhibit partial positive charge, and thus we expected that ligand **L7** could benefit both from the electron and polarization effect. Indeed, with R=Me, the naively designed ligand **L7** leads to a rather low OA barrier of 21.9 kcal/mol. On the other hand, the other two isomers, **L7_2** and **L7_N** both failed, due to the partial negative charge and the absence of HOMO distribution (and thus poor donor ability) on N, respectively. It is worth noting that **L7_2** is expected to be the privilege one if only the orbital effect is considered, since it is well-known that C2 owns the largest HOMO coefficient in the pyrrole ring. Therefore, this example again shows that the polarization effect could even outcompete electronic effect in some cases.

Taking **L7**(R=Me) as the starting point, we then further optimized it by replacing R with various

substituted aryl groups (Table S1), in order to subtly tune the electronic property of the ligand, and **L7**(R=2,6-difluorophenyl) was found to result in an even lower barrier, at 20.3 kcal/mol, which is 12797 folds faster than the original Nakao-type **L1**, and is expected to promote the OA reaction at room temperature.

We also explored the possibility of using counter-cations to tune the electrostatic and polarization effect, which leads to the design of **L8** (Figure 1 and Figure 6), an 18-crown-6 containing ligand. The capture of K^+ was expected to annihilate the lone pair on the *ortho*- and *meta*- oxygen, and thus inhibit the unwanted polarization stabilization of **Int1**. Indeed, in gas phase, **L8** leads to a rather low barrier of 20.2 kcal/mol.

With these privilege ligands designed in hand, we then examined their reactivity in solvation phase with moderate dipole (THF). Although the through-space polarization and electrostatic interaction may be reduced under polar solvents, we surprisingly found that the tendency above almost remains both even quantitatively (Figure 7). In THF solvation, the OA barrier for the original Nakao's **L1**(R1=R2=H) is slightly lower than in gas phase by 1.7 kcal/mol. The ligand **L1**(R1=NMe₂,R2=H), however, fails to give a lower barrier, indicating than simply introducing EDR at the *para*-site of Ring A not an good strategy in polar solvent. On the other hand, our strategy based on polarization effect remains quite efficient. The pyrrole based ligand **L7**, and crown ether containing **L8** both shows much lower barriers than **L1**. The anionic SO₃⁻ group was proven unnecessary: the NHC-potassium adduct **L9** also shows a low barrier of 22.8 kcal/mol, and this ligand might be easily prepared by adding salt into the crown ether containing neutral ligand complex. Overall, in this section we designed a bunch of potentially available new ligands guided by our rules above, and some of them were predicted to be much more reactive than the known analogues both in non-polar and moderately polar environment.

Barrier in THF (and gas phase in brackets)

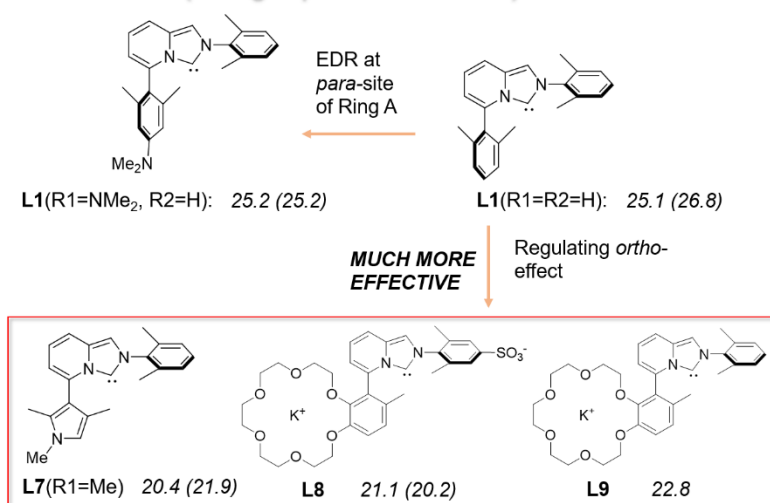


Figure 6. Structures and the corresponding OA barriers for selected ligands of interest with both geometry optimization and single point calculation under solvation of THF. The gas phase barriers are shown in brackets for comparison.

Conclusion

At this stage, we could make a summary and reclaim the rules for ligand design in Figure 1. With **L1** as a model for Nakao's NHC ligand, we studied the substituent effect on the NHC-Pd promoted OA reaction with 4-nitroanisole using the method of Hammett analysis. Ring A and Ring B were studied separately: for Ring B, the substituent effect is subtle, and both strong electron donating and strong electron withdrawing groups slightly lower the barrier. This effect is attributed to the dispersion interaction with the substrate phenyl group in the OA TS.

For Ring A, the *para*-substituent group exhibit a good Hammett linear relationship with the barrier. ETS-NOCV analysis shows that Ring A acts as a π -donor that stabilize the developing Pd(II) center, and thus strong EDR at the *para*- site stabilize the TS by increasing the donation to Pd. On the other hand, the substituent effect on *meta*- and *ortho*- site is rather complicated, and does not follow the order of any electronic effect. Although EDR at these sites still increases the donor ability of Ring A, the barrier is generally increased by these substitutions. This is concluded to be due to the polarization effect, which provides extra stabilization to the resting state: in the resting state **Int1** (the π -complex formed by Pd with substrate), the *ortho*- carbons, as well as the *ortho*-substituent groups themselves, bear electron density loss due to the polarization of nearby nitro group, and thus any factors that promotes polarization, such as the presence of n - or π - electron at these sites, will be harmful, and partial positive charge is expected to lower the barrier. This effect is in competition with another electrostatic effect, that any positive charge at these sites also interacts with the partial negative nitro group in **Int1**.

As a result, fine tuning of all these effects are demanded. The designed ligand in this work has shown that cationic motif should not be included as the *ortho*- substituent group on Ring A, because the electrostatic effect dominates then. However, properly-designed system, such as azulene rings or pyrrole rings containing ligands **L6** and **L7**, and crown ether containing ligand **L8** and **L9**, is shown to balance all the factors and give very low barriers. This work may provide both basic understanding and practical guideline for further ligand design, and we encourage experimentalists to try the pyrrole based or crown ether based ligands designed in this paper.

Methods:

The Gaussian 16 package²⁴ was employed to perform all the calculations, with the Gaussian 09 default integral grid. The PBE0 functional²⁵ was used in combination with the D3BJ correction^{26, 27}. For geometry optimization, the SDD ECP^{28, 29} and basis set were used for Pd, and 6-31G(d) basis set^{30, 31} was used for other elements. Frequency calculations were followed to ensure stationary points were found, and to obtain Gibbs free energy correction at room temperature. Single point calculations were performed with a larger basis set combination, in which the def2-TZVP³² and 6-311+G(d,p)^{33, 34} basis set were employed for Pd and other elements, respectively.

In order to validate our results in solvents with moderate dipole, both geometry optimization and single point calculation were repeated for the interested structures under SMD implicit solvation³⁵ of THF.

The ETS-NOCV analysis, electron density difference, IGM and ESP analysis were performed with the Multiwfn program³⁶.

Acknowledgement

Yumiao Ma thanks Hangzhou Yanqu Information Technology Co., Ltd for purchasing the license for Gaussian. Also thanks to all the students in Department of Chemistry, Tsinghua University, for their great love and encouragement toward Ma.

References:

1. Sambigioglio, C.; Marsden, S. P.; Blacker, A. J.; McGowan, P. C., Copper catalysed Ullmann type chemistry: from mechanistic aspects to modern development. *Chemical Society Reviews* **2014**, *43*, 3525-3550.
2. Heravi, M. M.; Kheilkordi, Z.; Zadsirjan, V.; Heydari, M.; Malmir, M., Buchwald-Hartwig reaction: an overview. *Journal of Organometallic Chemistry* **2018**, *861*, 17-104.
3. Farina, V., High-turnover palladium catalysts in cross-coupling and Heck chemistry: A critical overview. *Advanced Synthesis & Catalysis* **2004**, *346*, 1553-1582.
4. Kotha, S.; Lahiri, K.; DHURKE, K., Recent applications of the Suzuki–Miyaura cross-coupling reaction in organic synthesis. **2002**.
5. Suzuki, A., Recent advances in the cross-coupling reactions of organoboron derivatives with organic electrophiles, 1995–1998. *Journal of Organometallic Chemistry* **1999**, *576*, 147-168.
6. Nakao, Y.; Hiyama, T., Silicon-based cross-coupling reaction: an environmentally benign version. *Chemical Society Reviews* **2011**, *40*, 4893-4901.
7. Chinchilla, R.; Nájera, C., The Sonogashira reaction: a booming methodology in synthetic organic chemistry. *Chemical reviews* **2007**, *107*, 874-922.
8. Zhou, T.; Szostak, M., Palladium-catalyzed cross-couplings by C–O bond activation. *Catalysis Science & Technology* **2020**, *10*, 5702-5739.
9. Wang, L.; He, W.; Yu, Z., Transition-metal mediated carbon–sulfur bond activation and transformations. *Chemical Society Reviews* **2013**, *42*, 599-621.
10. Nakao, Y., Metal-mediated C–CN Bond Activation in Organic Synthesis. *Chemical Reviews* **2020**, *121*, 327-344.
11. Korch, K. M.; Watson, D. A., Cross-coupling of heteroatomic electrophiles. *Chemical reviews* **2019**, *119*, 8192-8228.
12. Shi, W.; Liu, C.; Lei, A., Transition-metal catalyzed oxidative cross-coupling reactions to form C–C bonds involving organometallic reagents as nucleophiles. *Chemical Society Reviews* **2011**, *40*, 2761-2776.
13. Kashiwara, M.; Nakao, Y., Cross-Coupling Reactions of Nitroarenes. *Accounts of Chemical Research* **2021**, 9423-9426.
14. Peng, L.; Hu, Z.; Tang, Z.; Jiao, Y.; Xu, X., Recent progress in transition metal catalyzed cross coupling of nitroarenes. *Chinese Chemical Letters* **2019**, *30*, 1481-1487.
15. Ono, N., *The nitro group in organic synthesis*. John Wiley & Sons 2003; Vol. 9.
16. Inoue, F.; Kashiwara, M.; Yadav, M. R.; Nakao, Y., Buchwald–Hartwig Amination of Nitroarenes. *Angewandte Chemie International Edition* **2017**, *56*, 13307-13309.
17. Yadav, M. R.; Nagaoka, M.; Kashiwara, M.; Zhong, R.-L.; Miyazaki, T.; Sakaki, S.; Nakao, Y., The Suzuki–Miyaura coupling of nitroarenes. *Journal of the American Chemical Society* **2017**, *139*, 9423-9426.
18. Nykaza, T. V.; Cooper, J. C.; Li, G.; Mahieu, N.; Ramirez, A.; Luzung, M. R.; Radosevich, A. T., Intermolecular Reductive C–N Cross Coupling of Nitroarenes and Boronic Acids by PIII/PV= O

- Catalysis. *Journal of the American Chemical Society* **2018**, *140*, 15200-15205.
19. Kashiwara, M.; Zhong, R.-L.; Semba, K.; Sakaki, S.; Nakao, Y., Pd/NHC-catalyzed cross-coupling reactions of nitroarenes. *Chemical Communications* **2019**, *55*, 9291-9294.
 20. Appleton, T.; Clark, H.; Manzer, L., The trans-influence: Its measurement and significance. *Coordination Chemistry Reviews* **1973**, *10*, 335-422.
 21. Hansch, C.; Leo, A.; Taft, R., A survey of Hammett substituent constants and resonance and field parameters. *Chemical reviews* **1991**, *91*, 165-195.
 22. Lefebvre, C.; Rubez, G.; Khartabil, H.; Boisson, J.-C.; Contreras-García, J.; Hénon, E., Accurately extracting the signature of intermolecular interactions present in the NCI plot of the reduced density gradient versus electron density. *Physical Chemistry Chemical Physics* **2017**, *19*, 17928-17936.
 23. Mitoraj, M. P.; Michalak, A.; Ziegler, T., A combined charge and energy decomposition scheme for bond analysis. *Journal of chemical theory and computation* **2009**, *5*, 962-975.
 24. Frisch, M. J.; Trucks, G. W.; Schlegel, H. B.; Scuseria, G. E.; Robb, M. A.; Cheeseman, J. R.; Scalmani, G.; Barone, V.; Petersson, G. A.; Nakatsuji, H.; Li, X.; Caricato, M.; Marenich, A. V.; Bloino, J.; Janesko, B. G.; Gomperts, R.; Mennucci, B.; Hratchian, H. P.; Ortiz, J. V.; Izmaylov, A. F.; Sonnenberg, J. L.; Williams; Ding, F.; Lipparini, F.; Egidi, F.; Goings, J.; Peng, B.; Petrone, A.; Henderson, T.; Ranasinghe, D.; Zakrzewski, V. G.; Gao, J.; Rega, N.; Zheng, G.; Liang, W.; Hada, M.; Ehara, M.; Toyota, K.; Fukuda, R.; Hasegawa, J.; Ishida, M.; Nakajima, T.; Honda, Y.; Kitao, O.; Nakai, H.; Vreven, T.; Throssell, K.; Montgomery Jr., J. A.; Peralta, J. E.; Ogliaro, F.; Bearpark, M. J.; Heyd, J. J.; Brothers, E. N.; Kudin, K. N.; Staroverov, V. N.; Keith, T. A.; Kobayashi, R.; Normand, J.; Raghavachari, K.; Rendell, A. P.; Burant, J. C.; Iyengar, S. S.; Tomasi, J.; Cossi, M.; Millam, J. M.; Klene, M.; Adamo, C.; Cammi, R.; Ochterski, J. W.; Martin, R. L.; Morokuma, K.; Farkas, O.; Foresman, J. B.; Fox, D. J. *Gaussian 16 Rev. C.01*: Wallingford, CT, 2016.
 25. Adamo, C.; Barone, V., Toward reliable density functional methods without adjustable parameters: The PBE0 model. *The Journal of chemical physics* **1999**, *110*, 6158-6170.
 26. Grimme, S.; Antony, J.; Ehrlich, S.; Krieg, H., A consistent and accurate ab initio parametrization of density functional dispersion correction (DFT-D) for the 94 elements H-Pu. *The Journal of chemical physics* **2010**, *132*, 154104.
 27. Grimme, S.; Ehrlich, S.; Goerigk, L., Effect of the damping function in dispersion corrected density functional theory. *Journal of computational chemistry* **2011**, *32*, 1456-1465.
 28. Martin, J. M.; Sundermann, A., Correlation consistent valence basis sets for use with the Stuttgart–Dresden–Bonn relativistic effective core potentials: The atoms Ga–Kr and In–Xe. *The Journal of Chemical Physics* **2001**, *114*, 3408-3420.
 29. Andrae, D.; Haeussermann, U.; Dolg, M.; Stoll, H.; Preuss, H., Energy-adjusted ab initio pseudopotentials for the second and third row transition elements. *Theoretica chimica acta* **1990**, *77*, 123-141.
 30. Hehre, W. J.; Ditchfield, R.; Pople, J. A., Self-consistent molecular orbital methods. XII. Further extensions of Gaussian-type basis sets for use in molecular orbital studies of organic molecules. *The Journal of Chemical Physics* **1972**, *56*, 2257-2261.
 31. Hariharan, P. C.; Pople, J. A., The influence of polarization functions on molecular orbital hydrogenation energies. *Theoretica chimica acta* **1973**, *28*, 213-222.
 32. Weigend, F.; Ahlrichs, R., Balanced basis sets of split valence, triple zeta valence and quadruple zeta valence quality for H to Rn: Design and assessment of accuracy. *Physical Chemistry Chemical Physics* **2005**, *7*, 3297-3305.

33. Francel, M. M.; Pietro, W. J.; Hehre, W. J.; Binkley, J. S.; Gordon, M. S.; DeFrees, D. J.; Pople, J. A., Self-consistent molecular orbital methods. XXIII. A polarization-type basis set for second-row elements. *The Journal of Chemical Physics* **1982**, *77*, 3654-3665.
34. Gordon, M. S.; Binkley, J. S.; Pople, J. A.; Pietro, W. J.; Hehre, W. J., Self-consistent molecular-orbital methods. 22. Small split-valence basis sets for second-row elements. *Journal of the American Chemical Society* **1982**, *104*, 2797-2803.
35. Marenich, A. V.; Cramer, C. J.; Truhlar, D. G., Universal solvation model based on solute electron density and on a continuum model of the solvent defined by the bulk dielectric constant and atomic surface tensions. *The Journal of Physical Chemistry B* **2009**, *113*, 6378-6396.
36. Lu, T.; Chen, F., Multiwfn: a multifunctional wavefunction analyzer. *Journal of computational chemistry* **2012**, *33*, 580-592.